



## Nonlinear interaction of energetic electrons with large amplitude chorus

J. Bortnik,<sup>1</sup> R. M. Thorne,<sup>1</sup> and U. S. Inan<sup>2</sup>

Received 28 July 2008; revised 22 August 2008; accepted 2 September 2008; published 6 November 2008.

[1] The effect of large amplitude chorus on energetic, radiation-belt electrons is evaluated using a general, relativistic, oblique, test-particle code. Three specific cases are examined: (A) Low-amplitude waves interacting at low-latitudes exhibit the expected, linear scattering which leads to large-scale diffusive behavior. (B) Large-amplitude waves interacting at low-latitudes result in monotonic decreases in pitch-angle and energy due to a resonance dislocation effect, leading to large-scale de-energization and particle loss. (C) Large-amplitude waves interacting obliquely at high latitudes result in a combination of the above behaviors, as well as nonlinear phase-trapping which leads to rapid, dramatic increases in both energy and pitch-angle of a small portion of the test-particles. These results suggest that the intensity of individual, discrete wave elements is critical for quantifying the large-scale dynamics of the radiation-belts. **Citation:** Bortnik, J., R. M. Thorne, and U. S. Inan (2008), Nonlinear interaction of energetic electrons with large amplitude chorus, *Geophys. Res. Lett.*, 35, L21102, doi:10.1029/2008GL035500.

### 1. Introduction

[2] The interaction of a single, charged particle with an electromagnetic whistler-mode wave in space, forms the fundamental building block upon which much of radiation-belt theory is predicated. For example, wave-particle interactions can cause energization and loss of outer radiation-belt electrons on short timescales [Thorne *et al.*, 2005; Horne *et al.*, 2005], leading to the formation of a low-L phase-space density peak [Green and Kivelson, 2004; Chen *et al.*, 2007].

[3] There are two basic theoretical approaches to describing the particle motion through the wave, involving (i) a direct manipulation of the Lorentz force equation [e.g., Inan *et al.*, 1978; Bell, 1984; Omura and Summers, 2006, and references therein], and (ii) a Hamiltonian formulation [e.g., Albert, 1993, 2002; Roth *et al.*, 1999]. Both approaches lead to the same set of ordinary differential equations (ODE's). For small amplitude waves, test-particles that are initially uniformly distributed in gyrophase spread in pitch-angle and energy diffusively [Inan, 1987; Albert, 2001]. However, for sufficiently large wave-amplitudes, the fundamental mode of wave-particle interaction can switch from being stochastic, to being deterministic, with an intermediate

region displaying dramatic examples of nonlinear behavior [Albert, 2002].

[4] Recent reports of large-amplitude whistlers [Cattell *et al.*, 2008; Cully *et al.*, 2008] raise questions of whether the traditionally-employed diffusion-based models are adequate for describing radiation-belt dynamics. In the remainder of this paper, we use a general test-particle formulation to examine three representative cases of wave-particle interaction, describe the 'resonance dislocation' effect, and place crude bounds on the regions of the three basic wave-particle interaction modes.

### 2. Simulation Details

[5] The dynamics of an electron, with rest mass  $m_e$  and charge  $q_e$  moving in an electromagnetic field are described by the Lorentz force equation:

$$\frac{d\mathbf{p}}{dt} = q_e \left\{ \mathbf{E}^w + \frac{\mathbf{p}}{m_e \gamma} \times [\mathbf{B}^w + \mathbf{B}_0(\lambda)] \right\} \quad (1)$$

where  $\mathbf{p} = m_e \gamma \mathbf{v}$  is the electron momentum,  $\gamma = (1 - v^2/c^2)^{-1/2}$ ,  $\mathbf{v} = d\mathbf{r}/dt$  is the particle velocity vector, and the total field has been separated into the wave components  $\mathbf{E}^w$ ,  $\mathbf{B}^w$ , and static geomagnetic field  $\mathbf{B}_0$ . Following the procedure of Bell [1984], (1) is rewritten as a set of three gyro-averaged ODE's, the first two describing the temporal evolution of the momentum parallel and perpendicular to the static magnetic field ( $dp_{\parallel}/dt$  and  $dp_{\perp}/dt$  respectively), and the third describing the evolution of the average phase angle  $\eta$  between the right-rotating component of the wave magnetic-field  $\mathbf{B}_R^w$  and  $v_{\perp}$ :

$$\frac{d\eta}{dt} = \frac{m\Omega}{\gamma} - \omega - k_{\parallel} \frac{p_{\parallel}}{m_e \gamma} \quad (2)$$

where  $m$  is the resonance harmonic number (+1 being the normal, counter-streaming resonance),  $\Omega$  is the local electron gyrofrequency,  $\omega$  is the wave frequency, and  $k_{\parallel} = k \cos \theta$  is the field-aligned component of the wave vector  $k$ , inclined at an angle  $\theta$  relative to  $-\mathbf{B}_0$ . The final equations are given by Bortnik [2004, equation (2.24)].

[6] Here, we study the wave-particle interactions at  $L = 5$  since this is the region where the largest amplitude chorus waves are present [Cully *et al.*, 2008], maximum inferred internal acceleration occurs [Green and Kivelson, 2004], and microbursts are most prevalent [e.g., O'Brien *et al.*, 2003], all presumably due to interactions with chorus. The magnetic field is assumed to be dipolar, varying only as a function of latitude. The plasma is assumed to be composed of electrons and ions, varying with latitude as  $n_e = n_{e0} \cos^{-4} \lambda$  [after Denton *et al.*, 2002] and  $n_{e0} = 10 \text{ cm}^{-3}$ .

<sup>1</sup>Department of Atmospheric and Oceanic Sciences, University of California, Los Angeles, California, USA.

<sup>2</sup>Space, Telecommunications, and Radioscience Laboratory, Stanford University, Stanford, California, USA.

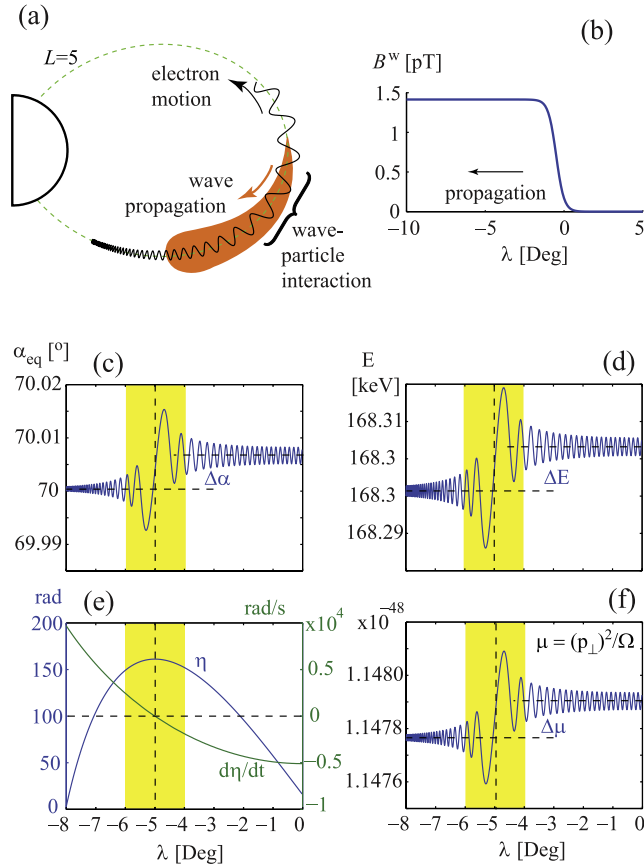


**Figure 1.** (a) Illustration of a wave-particle interaction at  $L = 5$ ; (b) wave propagation model; (c)–(f) equatorially-mapped pitch-angle of a single resonant particle; its total energy; phase angle  $\eta$  and rate of change  $d\eta/dt$ ; and first adiabatic invariant.

[7] Figure 1a illustrates the interaction between a chorus wave propagating away from the geomagnetic equator towards the southern hemisphere, and a northward-propagating electron ( $v_{\parallel} > 0$ ). The wave packet is taken to be static, monochromatic, and one-sided as shown in Figure 1b, described as  $B^w = B_0^w [\tanh(-2\lambda - 1) + 1]/2$ , where  $\lambda$  is latitude in degrees. Figures 1c–1f illustrate the interaction of a single test-particle with  $E_0 = 168.3$  keV,  $\alpha_{\text{eq}0} = 70^\circ$ , and  $\eta_0 = \pi$ , starting at an initial latitude of  $\lambda_0 = -9^\circ$ , with a field-aligned wave ( $\theta = 0^\circ$ ),  $B_y^w = 1$  pT (total  $B^w = 1.4$  pT), and  $f = 2$  kHz, propagating away from the equator. These parameters are chosen such that resonance (i.e.,  $d\eta/dt = 0$ ) occurs at  $\lambda = -5^\circ$ . Figures 1c, 1d and 1f show the evolution of the equatorially-mapped pitch-angle  $\alpha$ ,  $E$ , and the first adiabatic invariant  $\mu = p_{\perp}^2/\Omega$ . Each variable begins to oscillate as the particle approaches resonance  $d\eta/dt \sim 0$  (Figure 1e), indicated by the yellow block, at which point a permanent change is experienced by the particle, and  $\alpha$ ,  $E$ , and  $\mu$  are modified by  $\Delta\alpha$ ,  $\Delta E$ , and  $\Delta\mu$ , respectively.

### 3. Large Amplitude Scattering

[8] To illustrate the effect of large-amplitude whistler waves on the particles, we contrast three different cases, as shown in the three columns of Figure 2.

[9] Case A (Figure 2, column 1) shows scattering by small amplitude whistlers. The wave and particle parameters are similar to those of Figures 1c–1f, and the resonance location is set to  $\lambda_{\text{res}} = -5^\circ$ , to illustrate a typical low-latitude wave-particle interaction region. We simulate 24 test-particles, with initial phases  $\eta_0$  distributed uniformly between 0 and  $2\pi$ . Figures 2a and 2b show that  $\alpha_{\text{eq}}$  and  $E$  are scattered roughly symmetrically, and Figures 2c and 2d show that the total amount of scattering  $\Delta\alpha_{\text{eq}}$  and  $\Delta E$  is a sinusoidal function of  $\eta_0$  consistent with past work [e.g., *Inan et al.*, 1978]. The peak scattering in this single resonant interaction is proportional to the wave amplitude  $B^w$  (i.e.,  $\overline{\alpha_{\text{eq}}} = \sqrt{\langle (\Delta\alpha_{\text{eq}})^2 \rangle}$  and  $\overline{E} = \sqrt{\langle (\Delta E)^2 \rangle}$  grow linearly with time  $t$ ). If this same group of particles were to encounter successive resonances which are not phase-correlated to the first, the average particle scattering ( $\overline{\alpha_{\text{eq}}}$ ,  $\overline{E}$ ) would become diffusive, and proceed as  $\sqrt{B^w}$  (i.e.,  $\overline{\alpha_{\text{eq}}}$ ,  $\overline{E}$  grow linearly with  $\sqrt{t}$ ).

[10] Case B (Figure 2, column 2) demonstrates scattering by a large amplitude whistler. The parameters are identical to those of Case A, except that  $B_y^w = 1$  nT (i.e., total  $B^w = 1.4$  nT) corresponding to  $E^w \sim 50$  mV/m (for  $\theta = 0^\circ$ ) near the resonance location, consistent with the whistler intensities (0.5–2 nT) reported by *Cattell et al.* [2008]. All 24 test-particles are scattered to lower  $\alpha_{\text{eq}}$  and  $E$  ( $\Delta\alpha_{\text{eq}} \sim -5^\circ$  and  $\Delta E \sim -5$  keV), the changes are significantly larger than those in Case A, and the scattering is no longer a sinusoidal function of  $\eta_0$ . In this interaction, there is no energization of particles, unlike Case A. Since the trajectories of all particles are similar, we displayed one particle trajectory in black (Figures 2e and 2f) to aid in visibility.

[11] Case C (Figure 2, column 3) demonstrates scattering by large amplitude whistlers at high latitudes  $\lambda_{\text{res}} \sim 23^\circ$ , to reproduce the properties observed by *Cattell et al.* [2008]. We set  $n_{e0} = 3$  cm $^{-3}$  such that  $n_e(\lambda = 23^\circ) \sim 5$  cm $^{-3}$  (consistent with observations of 2–5 cm $^{-3}$ ),  $\theta = 50^\circ$  (observed range  $\sim 45^\circ$ – $60^\circ$ ),  $B^w \sim 1.4$  nT as in Case B (but  $E^w$  is now  $\sim 120$  mV/m, consistent with observations of 100–240 mV/m),  $E_0 = 500$  keV, and  $\alpha_{\text{eq}0} = 20^\circ$  so as to reach  $\lambda_{\text{res}}$ . The 24 test-particles were simulated for  $\sim 80$  ms (as in Cases A and B), consistent with the typical duration of a chorus wave packet. The wave frequency is 2 kHz (as before), consistent with *Cattell et al.* [2008], who observed the waves to be monochromatic. Since chorus that is field-aligned near the equator becomes more oblique as it propagates to higher latitudes, this case can also be viewed as the high-latitude extension of case B.

[12] As shown in Figures 2i and 2j, this case exhibits features that are not apparent in Cases A or B. The most dramatic difference is shown as a red trajectory, for a particle with  $\eta_0 = 7/12\pi$ , which becomes phase-trapped in the wave potential. Its energy is increased from a nominal 500 keV to  $\sim 800$  keV in 80 ms, and  $\alpha_{\text{eq}}$  is increased from  $20^\circ$  to  $\sim 60^\circ$ . The wave forces  $v_{\parallel}$  to vary in such a way that  $d\eta/dt$  returns to 0 repeatedly as opposed to a only single crossing (e.g., Figure 1e), thus effectively constraining  $v_{\parallel}$  to follow the resonant velocity  $v_{\parallel}^{\text{res}}$ , or alternatively, to move with the resonance island in the Hamiltonian formalism [*Albert*, 2002]. Of the 24 test-particles, only one other particle becomes phase trapped for a much shorter period of time, 3 particles gain some energy, and 19 particles of

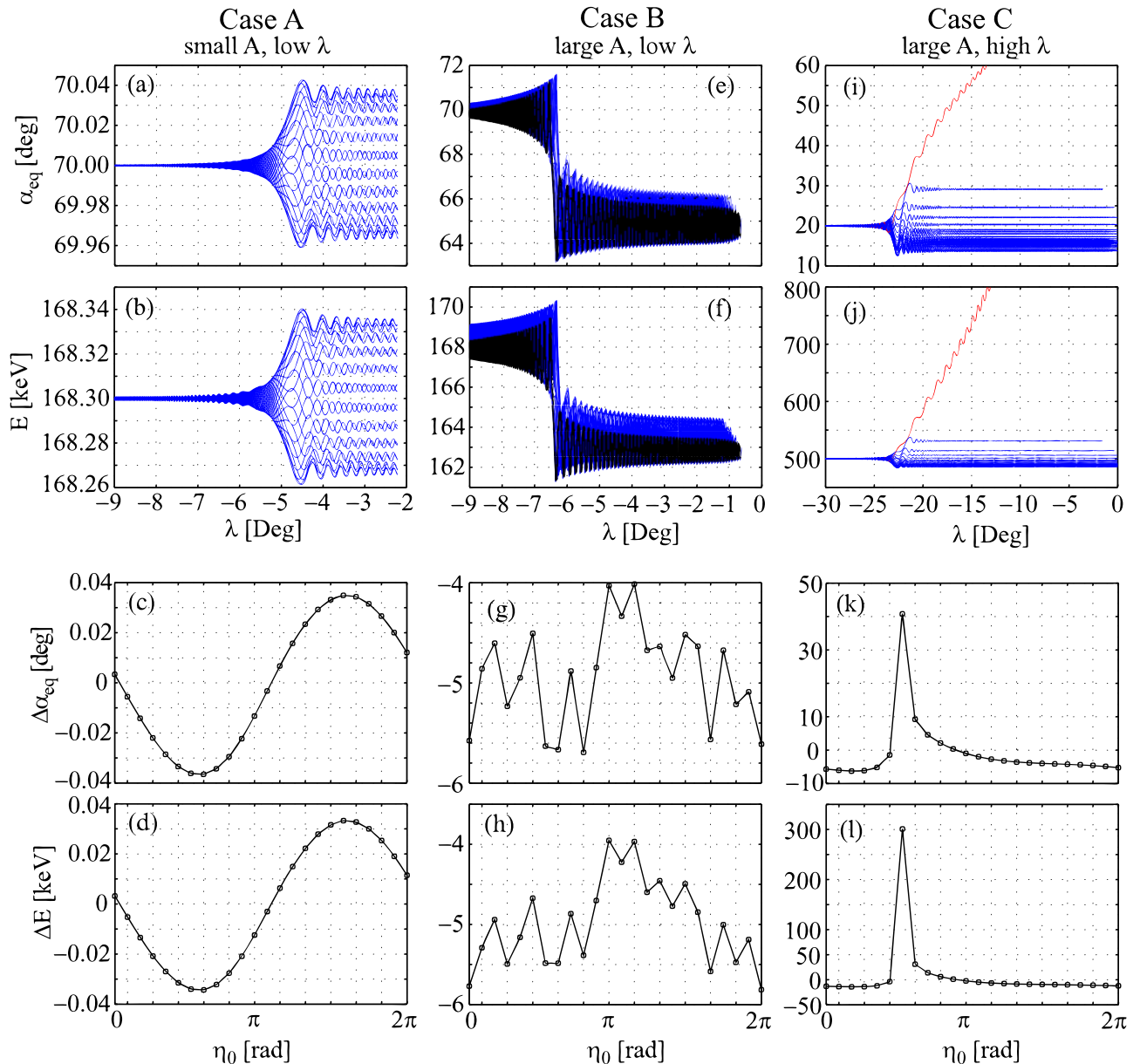


**Figure 2.** Test-particle interaction examples. Case A (Column 1), small-amplitude waves at low-latitude; Case B (Column 2), large-amplitude waves at low-latitude; Case C (Column 3), large-amplitude, oblique waves in low-density plasma, at high-latitudes. (a), (e), and (i) Equatorially-mapped pitch-angle; (b), (f), and (j) total energy in keV as a function of latitude; (c), (g), and (k) total pitch-angle change; and (d), (h), and (l) total energy change as a function of initial phase.

24 are shifted to lower pitch-angles and energies similarly to Case B. This case represents an intermediate situation between the small amplitude scattering of Case A, and the large amplitude scattering of Case B as discussed below.

#### 4. Discussion

[13] The results shown in Section 3 indicate that beyond a certain amplitude the wave-particle interaction changes qualitatively from that of diffusion and needs to be treated with a nonlinear approach. *Albert* [2002] identified three regimes of interaction which correspond to our simulated cases: a diffusive regime (Case A), phase-bunching regime (Case B), and a phase-trapping regime (Case C).

[14] The phase-bunching regime of Case B is illustrated in Figure 3a, where we show  $v_{\parallel}$  for two particles in Cases A and B in solid blue and green colors respectively ( $\eta_0 = \pi$ ). Setting  $d\eta/dt = 0$ , we calculate the corresponding resonant velocities using *Bortnik et al.* [2006, equation (2)], shown as blue and green dashed lines. Resonance for the small amplitude waves occurs at  $\lambda = -5^\circ$ , where  $v_{\parallel}$  intersects  $v_{\parallel}^{\text{res}}$ . However, for large-amplitude waves, the wave-induced oscillations in  $v_{\parallel}$  dominate the adiabatic variation in  $v_{\parallel}$ , such that the resonance condition is satisfied at a latitude of  $\sim -6.5^\circ$ . We call this forced change in resonance location a ‘resonance dislocation’ effect, which occurs when  $v_{\parallel}$  is increasing. During resonance, the value of  $\eta$  is temporarily

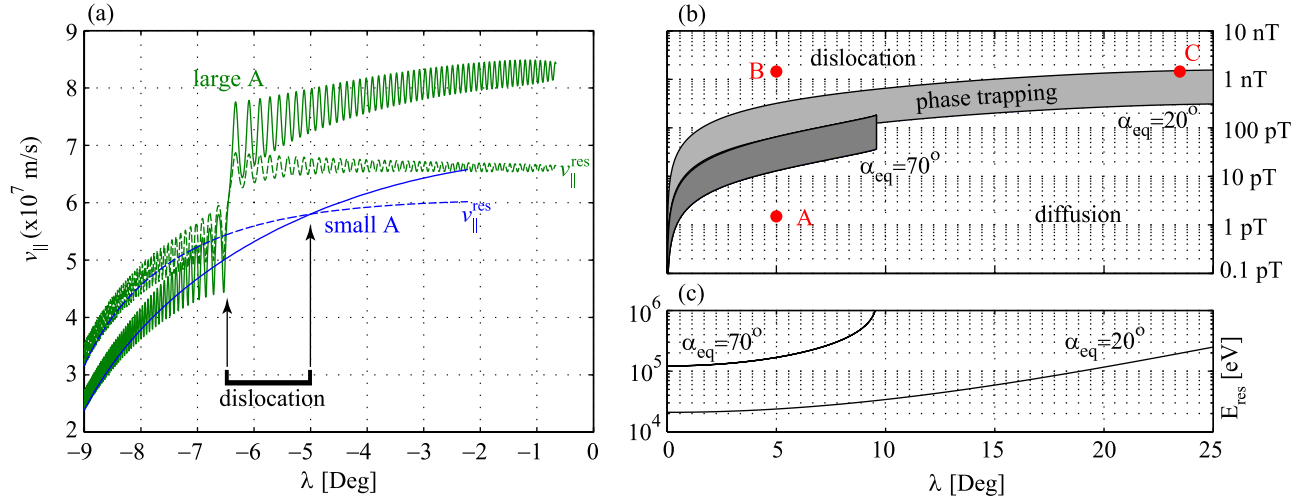


**Figure 3.** (a) Parallel velocity of a particle interacting at low-latitude with a small amplitude wave (solid blue line), and large amplitude wave (solid green line). Corresponding parallel resonant velocity shown in dashed blue and green lines respectively. (b) Linearity boundary for  $\alpha_{\text{eq}} = 20^\circ$  and  $\alpha_{\text{eq}} = 70^\circ$  electrons, for  $\rho = 1$  and  $\rho = 5$ . Superimposed in red circles are the parameters of Cases A–C in Figure 2. (c) Corresponding energies of particles in Figure 3b for  $\rho = 1$ .

held stationary such that  $v_{\parallel}$  continues to increase,  $\alpha_{\text{eq}}$  continues to decrease, and  $E$  decreases.

[15] The terms ‘small-amplitude’ and ‘large-amplitude’ waves, which we have used above, beg the question: small/large compared to what? The key quantities to compare, are the wave magnetic field  $B_w$ , against the static magnetic field inhomogeneity  $dB_0/dz$  [Inan *et al.*, 1978; Albert, 1993]. Below, we derive a simple expression based on [Inan, 1987, equation (9)] to estimate the linearity boundary, restricted to the case of field-aligned waves and non-relativistic particles. By dividing the pitch-angle into high and low ranges, the dimensionless parameter  $\rho$ , which is the ratio of the maximum absolute values of the oscillatory wave amplitude to the inhomogeneity forcing term, is simplified to:

$$\rho \approx \left( \frac{B_w}{dB_0/dz} \right) \left( \frac{2\Omega}{v} \right) \Gamma \quad (3)$$

where

$$\Gamma = \begin{cases} \left( 1 - \frac{\omega}{\Omega} \right) \frac{\sin \alpha}{3 \cos^2 \alpha}, & \alpha < 60^\circ \\ \frac{1}{\sin \alpha}, & \alpha > 60^\circ \end{cases} \quad (4)$$

When  $\rho < 1$ , the particle’s adiabatic motion (related to  $dB_0/dz$ ) dominates over the wave-induced motion (related to  $B_w$ ), and the wave-particle interaction can be viewed as a small, linear perturbation to the adiabatic trajectory. When  $\rho \gg 1$ , the wave-induced motion dominates over the adiabatic motion, and a completely non-linear interaction can be expected. However, in the transition region, when  $\rho > 1$ , the wave-induced motion and the adiabatic particle motion become comparable, and the interaction of these two forces can lead to extremely non-linear behavior such as phase-trapping, in addition to partially diffusive and nonlinear behavior.

[16] To quantify the linearity boundary, we evaluate (3) for the case of low ( $\alpha_{\text{eq}} = 20^\circ$ ) and high ( $\alpha_{\text{eq}} = 70^\circ$ ) pitch-

angle particles, at  $L = 5$ ,  $\lambda = 0^\circ - 25^\circ$  and plasma distributed as in Section 2 ( $n_{e0} = 10 \text{ cm}^{-3}$ ). The pitch-angle was mapped adiabatically to off-equatorial locations, and the resonant velocity was calculated at every point using (2). The results are shown in Figure 3b, where the region  $\rho < 1$  has been labeled ‘diffusion’, the region  $1 < \rho < 5$  is labeled ‘phase-trapping’ and  $\rho > 5$  is labeled ‘dislocation’. The corresponding resonant energy for the two curves is shown in Figure 3c. For reference, we have inserted the parameters of Cases A, B, and C onto Figure 3b (red circles), showing that they fall into the linear, nonlinear, and phase-trapping regions respectively. We also note that the obliquity of the wave, and the lowered plasma density used in Case C (but not Figure 3b) reduce the effectiveness of nonlinearity, and increase the linearity boundary, so Case C falls more strongly in the phase trapping region than appears. This also implies that oblique waves requires a larger amplitude to achieve the same level of phase-trapping as field-aligned waves.

[17] In general, lower  $\alpha_{\text{eq}}$  and higher  $E$  particles require larger  $B_w$  to achieve nonlinearity. Since  $B_w \propto dB_0/dz$ , the linearity boundary becomes vanishingly small near the equator  $dB_0/dz \rightarrow 0$ , so that even the smallest amplitude waves can produce nonlinear behavior. We note that in the configuration representative of chorus (wave propagating away from the equator), nonlinear dislocation always results in a lowering of both  $\alpha_{\text{eq}}$  and  $E$ , whereas phase trapping always results in a dramatic increase of both  $\alpha_{\text{eq}}$  and  $E$ , albeit for a small fraction of the resonant particles [Albert, 2002].

## 5. Conclusions

[18] Using a fully-relativistic, general, oblique-wave code, we have simulated the behavior of low ( $\alpha_{\text{eq}} = 20^\circ$ ) and high ( $\alpha_{\text{eq}} = 70^\circ$ ) pitch-angle particles, resonating at low ( $\lambda = 5^\circ$ ) and high ( $\lambda = 23^\circ$ ) latitudes, with small (1 pT) and large (1 nT) amplitude waves. These waves are modeled to be consistent with chorus, with a frequency of  $\sim 0.3\Omega_{\text{eq}}$ ,

propagating away from the geomagnetic equator. Results indicate that:

[19] 1. low amplitude waves resonating at low latitudes produce symmetrical scattering in both  $\alpha_{\text{eq}}$  and  $E$ , consistent with the underlying assumptions of quasilinear theory.

[20] 2. large amplitude waves resonating at low latitudes produce a deterministic, uniform decrease in both  $\alpha_{\text{eq}}$  and  $E$ , due to a highly nonlinear dislocation of the resonance point along the field-line.

[21] 3. large amplitude waves resonating at high latitudes can meet a condition where wave forces roughly balance adiabatic forces, resulting in the phase-trapping and nonlinear acceleration of a small number of particles, to large  $E$  and  $\alpha_{\text{eq}}$  over a timescale of  $\sim 80$  ms, comparable to a typical chorus element length.

[22] These results suggest that increasing the wave intensity does not necessarily increase the rate of diffusion as might be inferred from quasilinear theory. In fact, beyond the linearity boundary the wave-particle interaction can change its fundamental mode, and produce monotonic  $E$  and  $\alpha_{\text{eq}}$  decrease, or rapid energization for a small fraction of phase-trapped particles. The intensity of individual, discrete wave elements is thus a critical element in quantifying the large-scale dynamics of the radiation-belts and needs to be included in future radiation-belt models.

[23] **Acknowledgments.** JB and RMT acknowledge support from NSF grants ATM-0402615 and ATM-0621724 (GEM postdoc award) and NASA grants NNX08A035G and NNG04-G01G through subcontract 17496790-30026-A with Stanford University.

## References

- Albert, J. M. (1993), Cyclotron resonance in an inhomogeneous magnetic field, *Phys. Fluids B*, 5(8), 2744.
- Albert, J. M. (2001), Comparison of pitch angle diffusion by turbulent and monochromatic whistler waves, *J. Geophys. Res.*, 106(A5), 8477.
- Albert, J. M. (2002), Nonlinear interaction of outer zone electrons with VLF waves, *Geophys. Res. Lett.*, 29(8), 1275, doi:10.1029/2001GL013941.
- Bell, T. F. (1984), The nonlinear gyroresonance interaction between energetic electrons and coherent VLF waves propagating at an arbitrary angle with respect to the Earth's magnetic-field, *J. Geophys. Res.*, 89(A2), 905.
- Bortnik, J. (2004), Precipitation of radiation belt electrons by lightning-generated magnetospherically reflecting whistler waves, Ph.D. thesis, Stanford Univ., Palo Alto, Calif.
- Bortnik, J., U. S. Inan, and T. F. Bell (2006), Temporal signatures of radiation belt electron precipitation induced by lightning-generated MR whistler waves: 1. Methodology, *J. Geophys. Res.*, 111, A02204, doi:10.1029/2005JA011182.
- Cattell, C., et al. (2008), Discovery of very large amplitude whistler-mode waves in Earth's radiation belts, *Geophys. Res. Lett.*, 35, L01105, doi:10.1029/2007GL032009.
- Chen, Y., G. D. Reeves, and R. H. W. Friedel (2007), The energization of relativistic electrons in the outer Van Allen radiation belt, *Nature Phys.*, 3(9), 614, doi:10.1038/nphys655.
- Cully, C. M., J. W. Bonnell, and R. E. Ergun (2008), THEMIS observations of long-lived regions of large-amplitude whistler waves in the inner magnetosphere, *Geophys. Res. Lett.*, 35, L17S16, doi:10.1029/2008GL033643.
- Denton, R. E., J. Goldstein, and J. D. Menietti (2002), Field line dependence of magnetospheric electron density, *Geophys. Res. Lett.*, 29(24), 2205, doi:10.1029/2002GL015963.
- Green, J. C., and M. G. Kivelson (2004), Relativistic electrons in the outer radiation belt: Differentiating between acceleration mechanisms, *J. Geophys. Res.*, 109, A03213, doi:10.1029/2003JA010153.
- Horne, R. B., R. M. Thorne, S. A. Glauert, J. M. Albert, N. P. Meredith, and R. R. Anderson (2005), Timescale for radiation belt electron acceleration by whistler mode chorus waves, *J. Geophys. Res.*, 110, A03225, doi:10.1029/2004JA010811.
- Inan, U. S. (1987), Gyroresonant pitch angle scattering by coherent and incoherent whistler mode waves in the magnetosphere, *J. Geophys. Res.*, 92, 127.
- Inan, U. S., T. F. Bell, and R. A. Helliwell (1978), Nonlinear pitch-angle scattering of energetic electrons by coherent VLF waves in the magnetosphere, *J. Geophys. Res.*, 82(19), 127.
- O'Brien, T. P., K. R. Lorentzen, I. R. Mann, N. P. Meredith, J. B. Blake, J. F. Fennell, M. D. Looper, D. K. Milling, and R. R. Anderson (2003), Energization of relativistic electrons in the presence of ULF power and MeV microbursts: Evidence for dual ULF and VLF acceleration, *J. Geophys. Res.*, 108(A8), 1329, doi:10.1029/2002JA009784.
- Omura, Y., and D. Summers (2006), Dynamics of high-energy electrons interacting with whistler mode chorus emissions in the magnetosphere, *J. Geophys. Res.*, 111, A09222, doi:10.1029/2006JA011600.
- Roth, I., M. Temerin, and M. K. Hudson (1999), Resonant enhancement of relativistic electron fluxes during geomagnetically active periods, *Ann. Geophys.*, 17(5), 631.
- Thorne, R. M., T. P. O'Brien, Y. Y. Shprits, D. Summers, and R. B. Horne (2005), Timescale for MeV electron microburst loss during geomagnetic storms, *J. Geophys. Res.*, 110, A09202, doi:10.1029/2004JA010882.

J. Bortnik and R. M. Thorne, Department of Atmospheric and Oceanic Sciences, University of California, Los Angeles, CA 90095–1565, USA. (jbortnik@gmail.com; rmt@atmos.ucla.edu)

U. S. Inan, Space, Telecommunications, and Radioscience Laboratory, Stanford University, Packard Building, Stanford, CA 94305, USA. (inan@nova.stanford.edu)